The effects of topology upon fluid-flow and heat-transfer within cellular copper structures

J. Tian[*], T. Kim[*], T. J. Lu[*], H. P. Hodson[*], D. J. Sypeck[**] and H. N. G. Wadley[**]
[*]Department of Engineering, University of Cambridge
Trumpington St., Cambridge CB2 1PZ, UK
[**]Materials Science Department, University of Virginia
Charlottesville, VA 22903, USA
E-mail: jt289@cam.ac.uk ; tjl21@cam.ac.uk

Abstract

The fluid-flow and heat-transfer features of copper cellular metal structures made by the transient liquid phase (TLP) bonding of plane weave copper meshes (screens) were experimentally characterized under steady-state forced convection and compared with the performance of open cell copper foams. Due to the inherent structural anisotropy of a typical metal textile derived structure, the characterizations were performed for weaves configured in both the woven-screen (WS-A) and square-screen (WS-B) orientations, in order to identify the preferable orientation for maximizing thermal performance as heat dissipation media.

The experimental results for pressure drop and heat transfer were expressed on the basis of their representative unit cells. It was found that, at a fixed porosity (0.78), TLP bonded screen type WS-A has a slightly smaller Nusselt number but a much higher (~ 2.5 times) pressure drop per unit cell in comparison with that of WS-B. Comparisons with open cell copper foams suggest that wire-screen meshes compete favorably with the best available heat dissipation media. The overall thermal performance index (ratio of heat transfer to pressure drop) of TLP bonded wire-screens has a value approximately 3 times larger than that of copper foams with a stochastic structure but similar pore sizes, due mainly to the lower pressure drop encountered by the coolant flow during propagation through the periodic wire-screen structure.

Keywords: Forced convection, compact heat sinks, cellular metals, wire-screens

1. Introduction

High porosity, ultra-lightweight, cellular metal structures with open cell topologies have emerged in the past decade as attractive heat exchange media for a wide range of applications where dissipation of high intensity heat over relatively small spaces is demanded [1]. These cellular metal structures can be classified into two broad classes, one with a stochastic topology (i.e. metal foams) and the other with a periodic structure. A schematic illustration of the stochastic structures is shown in Fig. 1(a). Examples of the latter include materials made from stacked metal textiles [2] and microtruss concepts with tetrahedral, pyramidal, Kagome and other types of topologies [3]. A wide variety of process-routes have been developed to manufacture cellular metals with relative densities of 1-20% and cell sizes from 100μm to several centimeters [4]. The products differ greatly in quality and by three orders of magnitude in cost (the most costly are $12,000 per kg).

Several mechanisms contribute to hat transfer enhancements associated with the use of cellular metals, including interactions between the solid skeleton and a through-flowing fluid, and the importance of achieving a quality (low thermal resistance) metal-to-metal bond (brazing or transient liquid phase bonding is usually preferred over epoxy-bonding). Applications to electronics cooling and airborne multi-layer metal foam heat exchangers have been investigated, revealing promising

advances in the rate of heat removal [5].

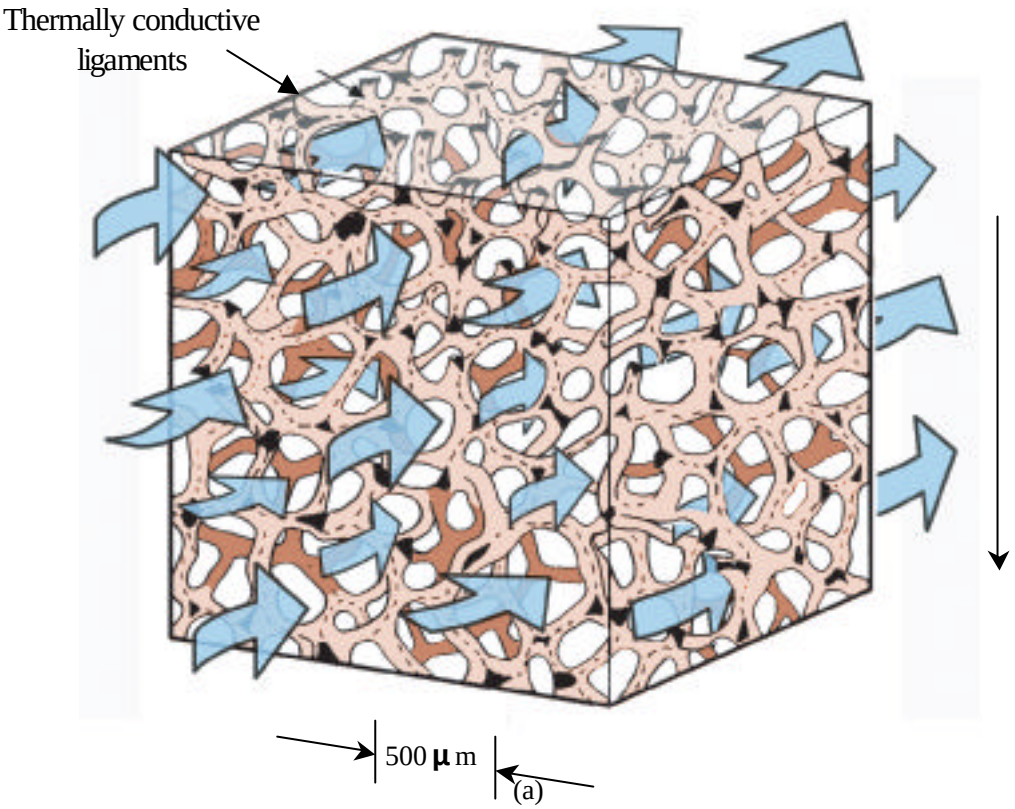

Fig. 1 (a) Schematic illustration of coolant flow across a stochastic structure; (b) topological comparison of periodic structures

While commercial metal foams with stochastic cellular morphologies are good compact heat exchangers and relatively cheap when made by sintering, they are not as structurally efficient as

periodic counterparts. This arises because their deformation under mechanical loading is dominated by cell wall bending as opposed to cell wall stretching [6]. Nonetheless, they are excellent cross flow heat exchangers because they provide a high thermal conductivity path for heat transport, a very high surface area for dissipation into a cooling fluid located in the pores and a contiguous path for forcing the coolant through the structure. Topologically configured ultra-light metals with periodic microtruss structures (tetrahedral, pyramidal, Kagome etc) have subsequently been developed (mainly by rapid prototyping or injection molding, followed by casting), which have good thermo-structural characteristics [2,7]. A topological comparison between different microtruss structures is made in Fig. 1(b). Their weight efficiency is as good as the best competing concepts, with additional multi-functionality advantages [7], but they are costly to manufacture by this route. The use of a metal textile technology coupled with novel bonding strategies to create periodic, cellular structures has the potential to improve the performance/cost ratio [2].

These metal textile derived cellular metals are the three-dimensional analogue of metallic textile screen meshes which have already been extensively used in fields such as aerospace, chemical product, food processing, air conditioning/refrigeration, and medicine [7]. Analytical models, backed with experimental measurements, have been developed to characterize the porosity, flow resistance, and heat transfer of wire screen meshes [8-14]. To meet the need for the design of heat pipes and Stirling engine regenerators, a number of studies have focused on predicting the effective thermal conductivity of fluid-saturated wire screens [9,10]. Duprat and Lopez [13] compared the thermal performance of three different heat regenerator media: monolith, stack of woven screens and a packed bed of spheres. Based on a given heat transfer efficiency, the energy efficiency of stacked wire-screens was found to cover a wider range of gauges. Ahmad et al. [14] studied the thermo-physical characteristics of various heat transfer media, and found that copper woven screens are promising thermal energy absorber matrices for packed-bed solar air heaters. Hsu et al. [15] developed an analytical model for the effective stagnant thermal conductivity of wire screens.

As far as heat transfer woven screen meshes is concerned, previous studies have focused on a single screen layer or self-supporting layers of screens stacked together without bonding. To the best of the present authors' knowledge, there has been no study on the effect of bonding wire-screens to create a three-dimensionally interconnected metallic network. Jiang et al. [16] carried out a combined experimental and numerical study on forced convective heat transfer in packed beds of sintered and non-sintered copper spheres, and found that, due to reduced thermal contact resistance, sintering can increase the overall heat transfer to a cross flowing fluid. The increases can be large- up to 15 times for water and 30 times for air. Here we explore the effects of bonding the nodes upon the thermal transport behavior. We note that such bonding also dramatically modifies the mechanical properties and creates opportunities for multifunctional applications of the type recently envisioned [1,6]. In this study, sandwich panels with woven-screen cores are fabricated by using a transient liquid phase (TLP) bonding method to create robust nodes at wire crossovers and between the laminae. The overall heat transfer performance of the panels under forced air convection is measured. Comparison with metal foams and microtruss materials is made.

2. Test Samples

2.1 Fabrication of heat exchangers

Two sandwich heat exchangers with laminated textile cores of plain square woven copper cloth (obtained from GDC / City Wire Cloth Co., Fontana, CA) were fabricated. The cloth was a 10 mesh with 0.635 mm diameter wires and a 1.905 mm opening. The wire alloy was C110000 copper (99.95Cu-0.04O) with a density $\rho_s = 8.89\ \mathrm{g/cm^3}$ and a thermal conductivity $k_s \approx 385$ W/(mK) at

ambient conditions. First, laminae were lightly sprayed with a mix of polymer based cement (Nicrobraz® Cement 520) and -140 mesh (diameter ≤ 106 mm) Ni-25Cr-10P braze alloy powder (Nicrobraz® 51), both supplied by Wal Colmonoy Corp. (Madison Heights, MI). The solidus and liquidus of this alloy are 880° C and 950° C whereas the melting point of copper is 1083° C. The coated laminae were then heated within flowing argon (at a vacuum level of approximately 10^{-1} Torr), at a rate of 20° C/min to 550° C to volatilize the polymer cement. An important feature of this braze/cement combination is that the braze alloy powders adhered to the wires after volatilization. The system was then evacuated to a vacuum level of less than 10^{-3} Torr and the temperature was ramped at a rate of 20° C/min to 1000° C and held there for 15 min. During this final heating, the braze alloy powders melted, coated the wires (this seals microscopic defects, if any), and the melt was preferentially drawn by capillary action to points of wire contact. This initial node rigidization procedure helps with more accurate stacking and alignment of multiple plies upon laminating. The rigidized laminae were again sprayed with the cement/powder mix and then stacked peak to peak (using pins to align all square openings). A small compressive pressure was applied to the periphery of the lay ups and the volitalization/heating procedure was repeated to construct the multi-laminate cores. The textile laminate cores had densities of approximately 1.8 g/cm^3 with corresponding relative densities of 20%.

The resulting samples had an anisotropic topology. When viewed perpendicular to the mesh, the structure had square openings with a relative large open area for fluid passage. Viewed from the side the individual layers formed a triangular pattern with significantly less open fluid passage. The sample sides were machined mutually orthogonal, with 0.813 mm thick copper facesheets attached. For one sample (Denoted screen A) the facesheets were coplanar with the meshes creating a situation where the fluid flow would be occurring through triangular channels (Fig. 2). For the second sample, the core was rotated so that flow occurred through the square channels of the structure. The facesheets were then sprayed and the volitalization/heating procedure was applied to metallurgically bond them to the cores. The solid facesheets are made of the same alloy as the wires.

For additional details see [2]. The sandwich panels created here can be designed to carry mechanical load at minimum weight, while simultaneously allowing fluid passage for cooling or other purposes.

2.2 Topology of textile core

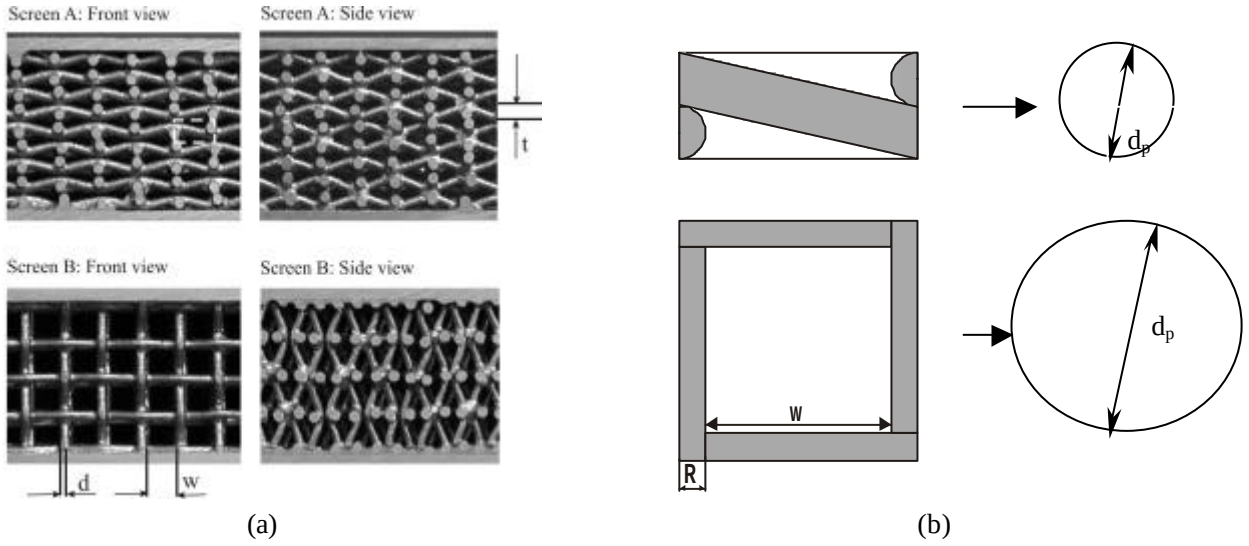

Fig. 2 Textile laminate heat exchangers: (a) images of two different screen meshes; (b) unit cell representation

Fig. 2 shows the topology of the two samples tested. The laminated textile cores are identical for

the two samples, except for their orientation relative to the face sheet. The laminated core is a typical orthogonal structure: the principal direction is along the aligned square pores, whereas the other two directions all have diamond-like shaped pores (not necessarily aligned). Both samples have width W=25 mm (the width of the testing channel), core height H=10 mm, face sheet thickness 1 mm, and length L=60 mm for wire screen A (WS-A) and L=50 mm for wire screen B (WS-B). For screen sample A, the trusses are all parallel to the faces, such that the passage of fluid flow is through the diamond-like shaped pores between stacked laminate. For screen sample B, the trusses are parallel and perpendicular to the faces, with flow directed along the aligned square pores.

2.3 Porosity and surface area density

The woven screens have a wire diameter $d = 0.635$ mm, width of square pore w = 1.905mm, and screen layer thickness $t = 2d$ (Fig. 2). The number of pores per unit length, N (mesh number), is:

$$N = \frac{1}{d + w} \tag{1}$$

For the present samples, N = 10 pores/in = 394 pores/meter. With ρ denoting the density of the screens, the relative density of a brazed square-mesh screen laminate can be calculated as [9]

$$\bar{\rho} \equiv \frac{\rho}{\rho_s} = \frac{\pi N d^2}{2(l/n)} \sqrt{1 + \left(\frac{1}{1 + w/d} \right)^2} \tag{2}$$

where n is the total number of screen layers, l is the total height of stacked layers, and the effect of bonding has been neglected.

As the screen layer is in a bed which can be either compacted or distended, its volume is determined by l/n instead of t. The square-root term in equation (2) is introduced to account for the effect of crimping of wires during weaving, with a value less than 1.03 when w/d > 3. The measured value of $\bar{\rho}$ is 0.22, slightly smaller than the value 0.21 predicted by (2), due to the added weight of bonding agent at contact points.

The porosity, ε, of the laminate is related to $\bar{\rho}$ by

$$\varepsilon = 1 - \bar{\rho} \tag{3}$$

Another mesh parameter importance for heat transfer analysis is the surface area density α_{sf} (total surface area per unit volume), given by

$$\alpha_{sf} = \frac{\text{total surface area}}{\text{unit volume}} = \frac{4(1-\varepsilon)}{d} \tag{4}$$

High surface area densities are desirable in creating the necessary interface properties for enhanced thermal transport in compact heat exchangers. The surface area density α_{sf} is governed by the number of pores per unit length, N. From equations (2) and (4), α_{sf} increases as the relative density is increased for a given wire diameter. With relative density fixed, α_{sf} decreases as the wire diameter is

increased. The value of a_{sf} can be engineered to exceed 2000 m^2/m^3 when N > 18 pores/in. This is comparable to the corresponding value of Duocell metal foams with similar pore sizes. It is larger than that of pin fin arrays and microtruss materials, making wire-screens potentially attractive as compact heat exchangers.

3. Experiments

3.1 Test set-up and data acquisition procedures

A schematic diagram of the test rig for pressure drop and heat transfer measurements is shown in Fig. 3. The main components are: air supply, test section, heating arrangement, and data acquisition. An open-circuit suction-type wind tunnel was constructed for this study. Ambient air, as coolant, is drawn into a rectangular Perspex channel (0.025 m width and 0.01 m height) containing the test section. Before reaching the test section, efforts were made to ensure the coolant flow was fully developed. To achieve this the coolant first flows through a wire screen layer (wire diameter = 0.56 mm), followed by a 4:1 contraction section, a honeycomb layer, another wire screen layer, and a long parallel plate channel (with a ratio of section length to channel height, *L1/H*=35).

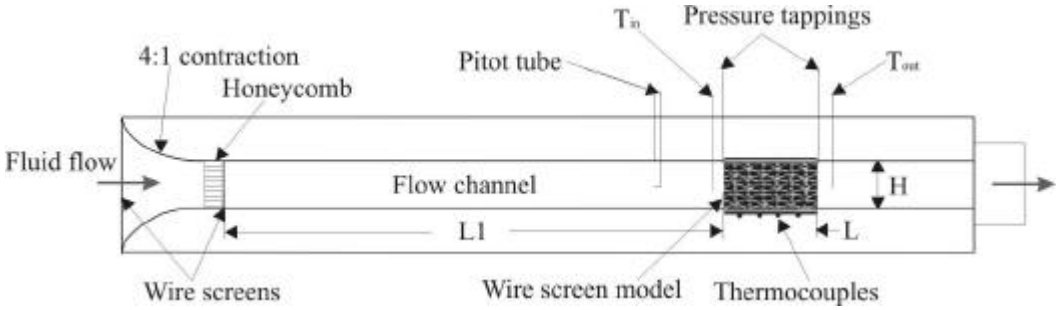

Fig. 3 Forced air convection test rig

A Pitot tube was placed at the center and adjacent wall pressure tapping was used for maximum flow velocity measurement. The ratio of channel height (10 mm) to outer tube diameter (0.51 mm) of the tube, is 19.6. The wall interference on the Pitot tube is expected to be negligible. The inlet coolant velocity profile over the channel height was measured to get the mean flow velocity. For pressure drop measurements, two static pressure tappings monitored by a digital manometer were positioned at the inlet and outlet of the test section, respectively.

Table 1 Experimental operating conditions

Parameters	Ranges
Inlet coolant velocity	1.0~10m/s
Reynolds number Re_{dp}	WS-A: 150~1200 WS-B: 250~2000
Heat flux	430622 W/m^3
Inlet temperature	290.0 K
Outlet temperature	300.0 ~320.0 K

For the heat transfer measurement, an isoflux (constant wall heat flux) boundary condition was imposed on the bottom face sheet of the test sandwich by a heating pad (silicone-rubber etched foil from Watlow^{TM} Inc.), whilst the top face sheet is thermally insulated. A pure copper heat spreader plate, 0.9 mm thick, was inserted between the heating element and the bottom face sheet of the wire-screen sandwich to ensure the uniformity of the heat flux. Four thin (0.013 mm thickness) T-type copper-constantan foil thermocouples (butt bonded) were mounted onto the bottom face sheet along the centerline in the flow direction. Two additional T-type bead thermocouples were positioned separately at the inlet and outlet of the test section to measure the coolant temperature at mid-height at

each location. All measurements were performed under steady state conditions and repeated until significant data repetition was ensured, i.e., 5% uncertainty interval (see measurement uncertainties discussed below). The test conditions are listed in Table 1.

3.2 Data reduction parameters

Experimentally, Kim et al. [17] observed that in an open-celled metal foam with a typical stochastic structure, fluid flows in repeated patterns over blocks of foam cells (excluding those near the entrance and exit regions), and hence information obtained from a representative unit cell can be utilized to describe the whole structure. The pressure loss coefficient and Nusselt number defined on the basis of a unit cell have been successfully used by Kim et al. [17] to correlate a multitude of test data from metal foams with different morphological features (pore size, porosity, etc.). A similar approach is used in the present study to treat periodic wire-screen structures shown in Fig. 2(a). Fig. 2(b) illustrates that the unit cell size for both samples is determined in the same way as that used to determine the hydraulic diameter of an open channel. In other words, a circular cell with diameter d_p has the same frontal area of the representative unit cell. For WS-A, $d_p = 1.28$ mm, and for WS-B, $d_p = 2.15$ mm.

The dimensionless Reynolds number and pressure loss coefficient based on the unit cell length are defined as:

$$\mathrm{Re}_{dp} = \frac{\rho U_m d_p}{\mu} \tag{5}$$

$$K_{Cell} = \frac{\Delta P_{Cell}}{\rho U_m^2 / 2} = \left(\frac{\Delta P}{L} \cdot d_p \right) \cdot \left(\frac{1}{\rho U_m^2 / 2} \right) \tag{6}$$

where U_m is the mean coolant velocity at the inlet of the test section, ΔP_{Cell} is static pressure drop per unit cell length ($= \Delta P \cdot d_p / L$), $\Delta P / L$ is pressure drop per unit length, and ρ is the density. To calculate the overall pressure drop across the wire-screen heat exchanger, K_{Cell} needs to be multiplied by the total number of pores in the flow direction. The mean inlet coolant velocity is between 1.0m/s to 10m/s, which includes laminar flow and turbulent flow. The lower bound of coolant velocity was set by the stability of coolant flow whilst the upper bound was limited by pumping capacity.

For heat transfer characterization, the volumetric heat transfer coefficient h_v and the corresponding Nusselt number Nu_{dp} are defined as:

$$h_v = \frac{q}{T_w - T_{f,bulk}} \tag{7}$$

$$Nu_{dp} = \frac{h_v d_p^2}{k_f} \tag{8}$$

where the coordinate x measures from the entrance of the testing sample in the main flow direction, k_f is the thermal conductivity of the coolant. $q = Q/V$ is input heat flux. Here, Q is the heat input, V is the volume of wire screen, T_w is temperature of the bottom face sheet, and $T_{f,bulk}$ is bulk mean temperature of the coolant at inlet.

3.3 Measurement uncertainty

An uncertainty analysis was performed by using the method described in Coleman and Steele [18]. The maximum heat loss through insulation materials was estimated to be less than 2% of the total input heat. The variation in the thermal conductivity of air, k_f, is negligible in the operating temperature range of 300 K to 330 K (maximum), whereas its density varies by about 5%. The uncertainty in pressure drop measurement was estimated to be less than 5%. The uncertainties calculated from the root-square method for the mean heat transfer coefficient, Reynolds number and Nusselt number were estimated to be less than 5.3%, 5.7% and 5.4%, respectively.

4. Results and Discussion

The brazed wire-screens are structurally periodic and deterministic but anisotropic. As described in section 2.2 and seen in the front views of Fig. 2, orientation A has completely different flow passages in comparison with orientation B. The flow passages in the former are staggered and the pores are diamond-like in shape, whilst in the latter the flow passages are more open and the pores are square. Therefore, it would be interesting to compare the thermal and hydraulic of the two wire-screen samples with identical porosity ($e = 0.78$). The measured pressure loss coefficients, Nusselt numbers, and efficiency indices of the two samples will also be compared with those of copper metal foams with stochastic morphology [17]. The relevant parameters of all of the tested samples are summarized in Table 2.

Table 2 Parameters of morphology for all samples

Samples	**Properties**				
		Screen A		Screen B	
Brazed wire screens	Porosity, ε	0.78		0.78	
	Unit cell length, d_p(mm)	1.44		2.78	
		S-9	S-10	S-11	S-12
Sintered copper foams	Porosity, ε	0.933	0.918	0.956	0.900
	Unit cell length, d_p(mm)	2.645	2.697	1.284	1.431

4.1 Pressure loss

Compact heat exchangers are expected to have high rate of heat transfer with a low pressure drop. The pressure loss coefficient K_{Cell}, defined in equation (6), was plotted against Reynolds number Re_{dp} in Fig. 4. When $Re_{dp} < 150$ for WS-A (for WS-B, $Re_{dp} < 350$), the flow is laminar. In laminar flow regime, the pressure loss coefficient K_{Cell} decreases with increasing Re_{dp}. At high Reynolds number, the pressure loss coefficient K_{Cell} is nearly constant. That is, K_{Cell} is independent of Reynolds number in turbulent flow regime. At a given Reynolds number, K_{Cell} of WS-B is much lower than that of WS-A. That means that the resistance encountered by the flow in orientation of WS-A is much higher than that in WS-B. In the turbulent regime, the pressure loss coefficient of WS-A ($K_{Cell} = 4.35$) is about 2.35 times that of WS-B ($K_{Cell} = 1.85$). In the current study of TLP

bonded wire screens, the porosity is fixed ($\varepsilon = 0.78$), and from the front view of two samples, it showed that the flow passages of two samples are different. It is clear that the pressure loss coefficient is strongly dependent upon the contribution blockage. In order to quantify the contribution of blockage effect on pressure drop, the blockage ratio is defined as

$$R_{BR} = 1 - \frac{open \quad area}{total \quad area} \tag{10}$$

The blockage ratio (0.75) of sample WS-A is nearly twice that of sample WS-B (0.37). Consequently, the measured pressure drop across WS-B is significantly lower than that across WS-A, implying that the pressure loss in the current range of fluid-flow is mainly attributable to the pressure difference-related form drag across the wire-screens. In general, K_{Cell} increases as the blockage ratio is increased. K_{Cell} is a function of R_{BR}, $K_{Cell} \propto f(R_{BR})$.

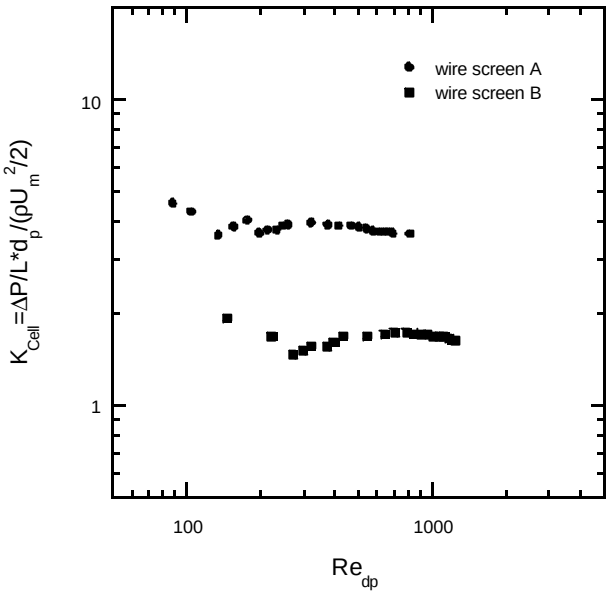

Fig. 4 Pressure loss coefficient as a function of Reynolds number of wire screens

Fig. 5 compares the pressure loss coefficients of copper wire screens with those of copper foams [17]. In order to examine the effect of porosity, comparisons are made between two groups of samples with similar pore sizes but different porosities: (a) WS-A (ε = 0.78, d_p = 1.28 mm) and foam samples S-11 (ε = 0.956, d_p = 1.284 mm) and S-12 (ε = 0.900, d_p = 1.431 mm); (b) WS-B (ε = 0.78, d_p = 2.15 mm) and foam sample S-9 (ε = 0.933, d_p = 2.645 mm) and S-10 (ε = 0.918, d_p = 2.697 mm). At the similar pore size, the pressure loss coefficient K_{Cell} of foams increases with decreasing porosity. K_{Cell} is also a function of porosity, $K_{Cell} \propto f(1-\varepsilon)$. Compared these two structures, even the porosity of wire screens is much lower that those of copper foams, the pressure loss coefficient is still smaller than copper foams' . The pressure loss coefficient of WS-A is close to copper foam S-11 and smaller than S-12. For WS-B, K_{Cell} is much smaller than S-09 and S-10.

Kim et al. [17] found that the pressure loss coefficient of an open-celled metal foam increases with decreasing porosity, and the empirical correlation $K_{Cell} = B(1-\varepsilon)^{3/2}$ describes the tests data well in the turbulent regime, where B is an empirical (dimensionless) constant. As mentioned above, the pressure loss coefficient of wire screens depends on not only the porosity, but also the blockage ratio. The same conclusion was reached in the case of aluminum microtruss (lattice-frame) materials

($e = 0.94$) consisting of a three-dimensional network of cylindrical struts [19]. For periodical structures such as wire screens and truss cored materials, the blockage ratio R_{BR} can be straightforwardly calculated based on geometry analysis. For metal foams having stochastic structures, a similar geometrical analysis is yet to be performed. However, for both periodic and stochastic structures, it is anticipated that the pressure loss coefficient can be expressed as a function of porosity and blockage ratio as $K_{Cell} = B_0(1-e)^{3/2} f(R_{BR})$, where B_0 is a non-dimensional constant. The relationship between K_{Cell} and R_{BR} needs further investigation.

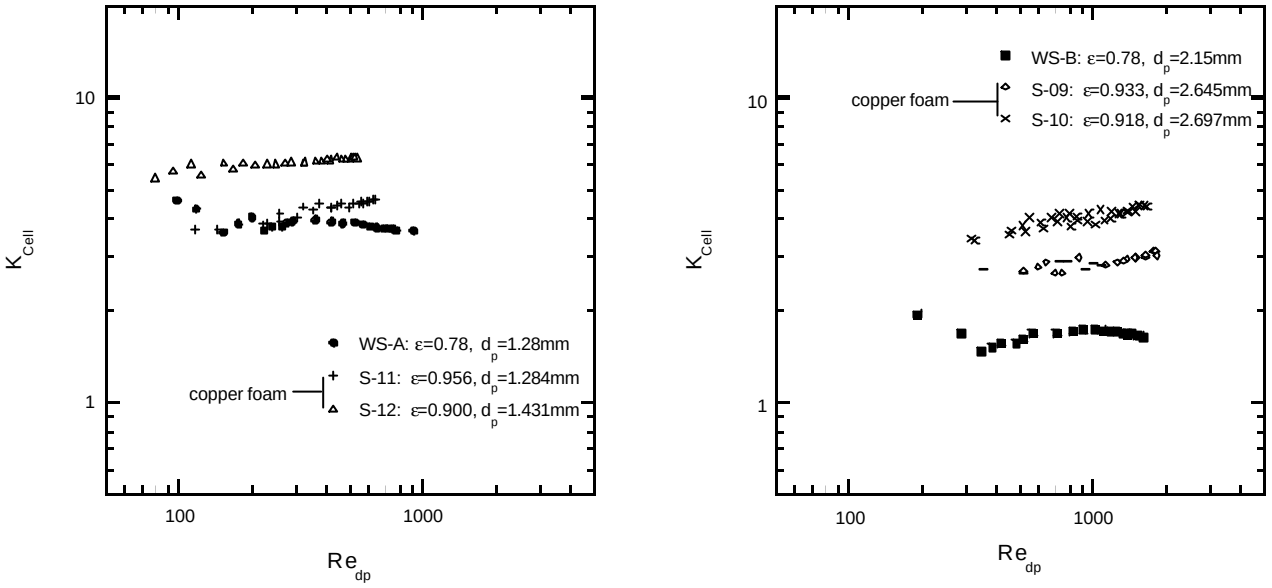

(a) (b)

Fig. 5 Comparison of pressure loss coefficient with open-celled copper foams (similar cell sizes) (a) WS-A with copper foam sample S-11 and S-12; (b) WS-B with copper foam sample S-9 and S-10

4.2 Heat transfer performance

The unit-cell based Nusselt number of both wire-screen samples is plotted against the Reynolds number in Fig. 6. Both sets of data can be well correlated by

$$Nu_{dp} = C \cdot (\mathrm{Re}_{dp})^n \qquad (11)$$

where *C* and *n* are dimensionless constants; their values are summarized in Table 3.

Table 3. Empirical correlation of the brazed wire-screens, the sintered copper foams based on mean pore diameter

Samples		**C**	**n**
Brazed wire-screens	A	1.0972	0.4705
	B	2.7705	0.5341
Sintered copper foams	S-09	0.9218	0.7418
	S-10	0.4253	0.8255
	S-11	0.1233	0.9743
	S-12	0.0807	0.9680

It is interesting to see from Fig. 6 that sample WS-B has a larger Nusselt number at a given

Reynolds number than that of WS-A, even though its pressure loss coefficient is smaller than the latter. Also, the heat transfer rate of WS-B increases slightly faster than WS-A as the Reynolds number is increased (Fig. 6). From the study of bank of cylinders, the flow after one cylinder depends on the arrangement of cylinders. If the distance of two rows of cylinder is too close, the vortex after the first row hasn't completed yet when the new vortex starts. If the distance is long enough for vortexes to complete, the flow is less turbulent. From the side view of two wire screen samples in Fig. 3(a), the cell length along the flow direction of WS-B is shorter than that of WS-A. The flow inside of WS-B may be more turbulent than that of WS-A. Then, more turbulent flow takes more heat away, and hence, the heat transfer performance is better. This needs to be proved. This is a limiting case due to the low thermal conductivity of the cooling, air.

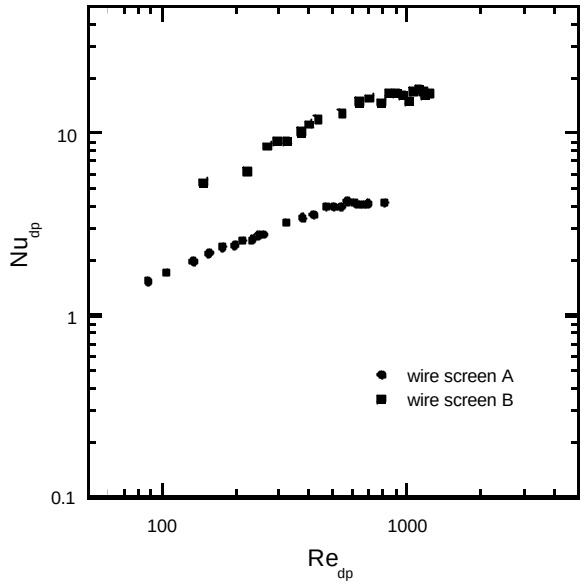

Fig. 6 Nusselt number as a function of Reynolds number

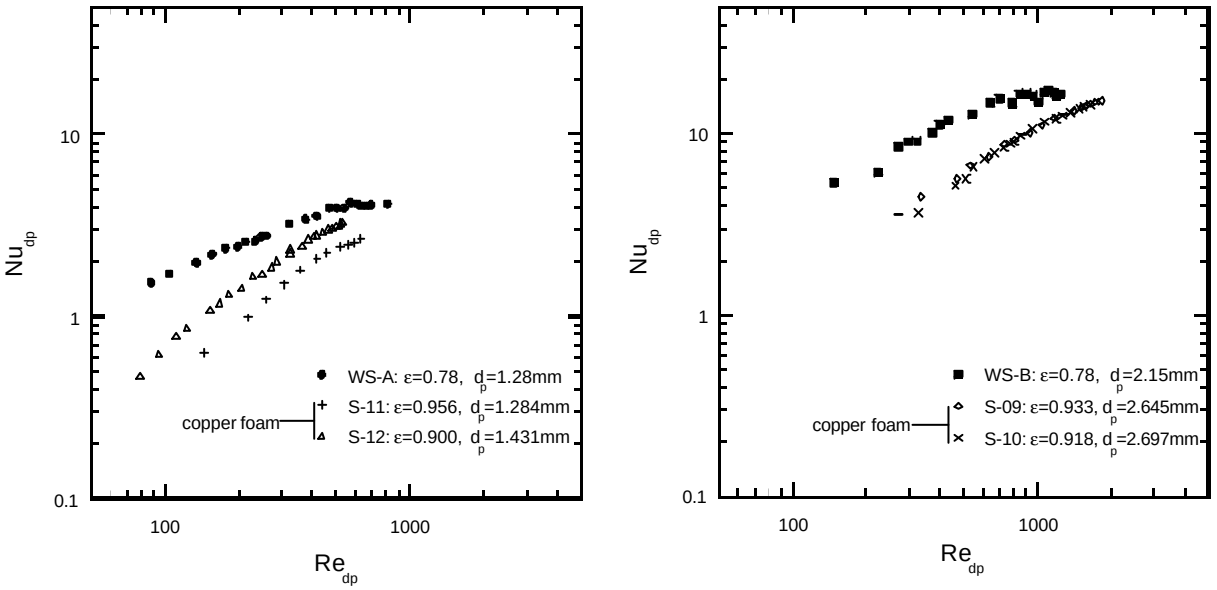

(a) (b)

Fig. 7 Comparison of Nusselt number with open-celled copper foams having similar cell sizes
(a) WS-A with copper foam sample S-11 and S-12; (b) WS-B with copper foam sample S-9 and S-10

Comparison with copper metal foams having different porosities and similar pore sizes is

shown in Fig. 7. Heat dissipation in these highly porous materials is controlled mainly by solid conduction, convection, thermal dispersion, and thermal contact resistance between face sheet and core. Because of the high conductivity of copper and low conductivity of air, the effect of thermal dispersion is negligible [20]. With the similar pore size, the sample with higher porosity has better heat transfer performance.

Due to the complexity associated with parametric studies in heat transfer as well as the lack of experimental data for wire-screens, the correlation between heat transfer and morphological/physical parameters such as porosity, surface area density and solid thermal conductivity will be carried out in a future study.

4.3 Overall thermal efficiency

A good heat exchanger has a high rate of heat exchange but low pressure-drop. Heat exchanger design parameters such as heat transfer coefficient and pressure drop should be simultaneously considered when studying overall thermal efficiency. A non-dimensional thermal efficiency index is thus introduced as:

$$I_{Cell} = j_{dp} / K_{Cell} \tag{12}$$

where $j_{dp} = \mathrm{Nu}_{dp}\,\mathrm{Re}_{dp}^{-1}\,\mathrm{Pr}^{-1/3}$ is the j-Colburn factor. Fig. 8 compares the overall thermal performance of the two wire-screen samples in terms of I_{Cell}. For the range of Reynolds number considered, WS-B has a I_{Cell} value approximately 10 times that of WS-A, due mainly to the lower pressure drop in the former case.

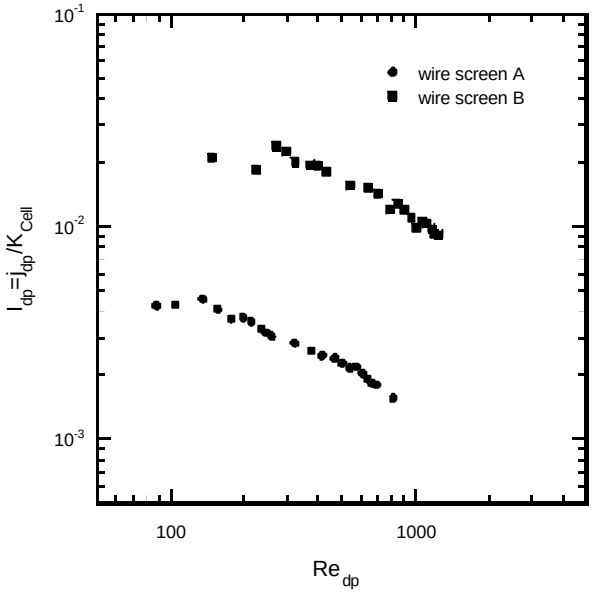

Fig. 8 Thermal efficiency index as a function of Reynolds number

The results of comparison between wire screens and copper foams are plotted in Figs. 9(a) and 9(b), respectively. Clearly, the overall thermal performance of wire screens is much better than that of foams having similar cell sizes but higher porosity levels. At a given Reynolds number (Re_{dp}=500), I_{Cell} of WS-A is around 2 times of copper foam sample S-11 and S-12; I_{Cell} of WS-B is around 5 times of copper foam samples S-09 and S-10. The difference would slightly decrease if the data for metal foams were extrapolated to the same porosity (0.78) as that of wire-screens [2, 20]. The

superiority of periodic wire screens over stochastic metal foams stems mainly from their low pressure loss, and hence the overall thermal performance of a compact heat exchanger can be enhanced by designing its microstructure (geometry and pore shape) against minimum pressure loss while maintaining other parameters such as porosity and pore size unchanged.

Comparisons with truss materials [19] have also been made, and it is found that the heat dissipation capability of wire-screens is an order of magnitude higher simply because for the truss materials studied [19], the truss dimensions are such that their surface area density is an order of magnitude smaller than that of wire-screens. It is anticipated that the heat transfer performance of wire-screens, metal foams and truss materials will be similar if they all have the same surface area density: the major difference will stem from their pressure drop due to different fluid passage patterns. Certainly, a systematic optimization would require a concerted study on the effects of all relevant morphological parameters.

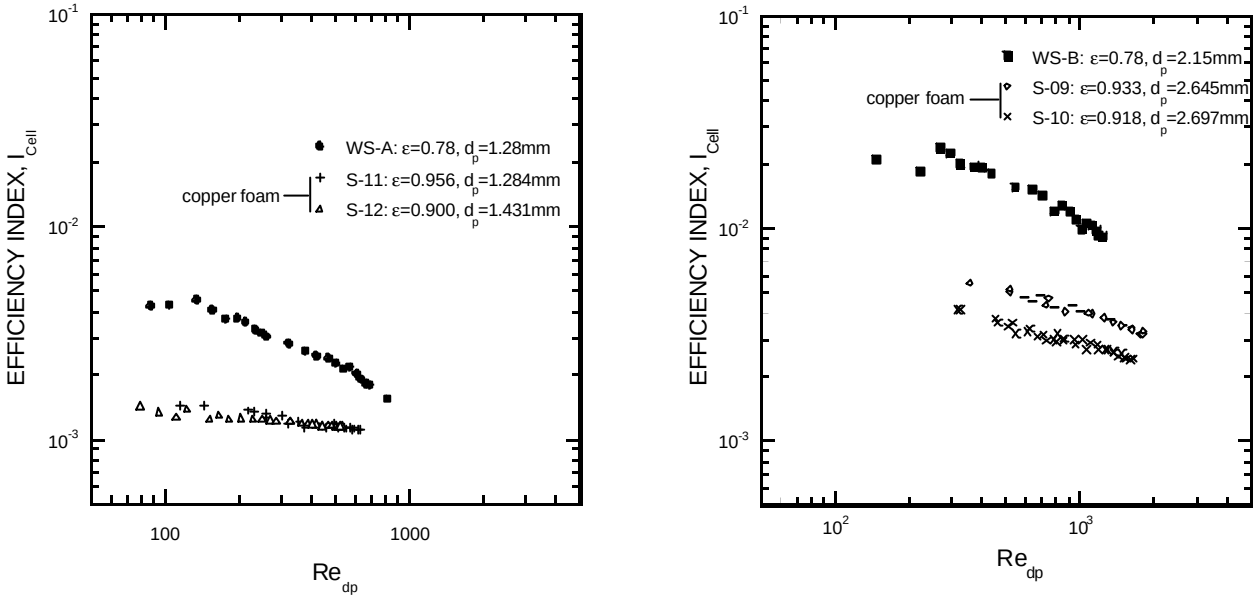

Fig. 9 Comparison of thermal efficiency indices between wire screens and copper foams
(a) WS-A with copper foam sample S-11 and S-12; (b) WS-B with copper foam sample S-9 and S-10

5. Conclusions

The pressure drop, volumetric heat transfer, and overall thermal performance of TPL bonded wire-screen meshes have been experimentally investigated under steady-state forced convection conditions. Two screen types with different flow passages but identical porosity were tested, with uniform heat flux boundary condition imposed. Screen type WS-A is staggered and has diamond-like shaped pores, whereas screen type WS-B has more open passages of flow with square shaped pores. For the range of Reynolds number (based on unit cell) considered, fluid flow in both screen meshes is turbulent: that is, pressure loss coefficient in both cases is independent of coolant velocity. However, the pressure drop in WS-B is about 60% smaller than that in WS-A, because its blockage ratio is less than that of WS-A. The pressure loss coefficient is a function of porosity and blockage ratio.

Comparisons made between copper wire-screens and open-celled copper foams show that, thermally, the wire-screens are as good as metal foams, both having large surface area densities. However, the pumping power required is significantly smaller for wire-screens. The overall thermal performance index (ratio of heat transfer to pressure drop) of wire-screens has a value approximately 2~5 times larger than that of copper foams with stochastic structure but similar pore sizes, due mainly to the low pressure drop encountered by the coolant flow across the periodic wire-screen structure.

Significant opportunities to maximize the heat transfer performance of periodic cellular metals by varying the pore fraction, anisotropy of the pores and metallic alloy used appear to exist. Such manipulation can be accomplished by selection of the appropriate wire mesh.

Acknowledgements

This work was supported by the U.S. Office of Naval Research through ONR/ONRIFO grant number N000140110271 and ONR grant number N000140010342 (program manager, Dr Stephen Fishman), and by the U.K. Engineering and Physical Sciences Research Council (EPSRC grant number EJA/U83).

Nomenclature

B, B_0	Empirical constants
C, C_0	Empirical constants
c_p	Coolant specific heat
d	Wire diameter [m]
d_p	Pore diameter [m]
D_h	Hydraulic diameter (=2WH/(W+H)), [m]
H	Height of testing sample [m]
h_v	Volumetric heat transfer coefficient [kW/m^{3}K]
L	Length of testing sample [m]
l	Total height of stacked layers [m]
I	Efficiency index, $I=j_{dp} / K_{Cell}$
j_{dp}	Colburn j factor, ($j_{dp}=Nu_{dp}Pr^{-1/3}/Re_{dp}$)
K_{Cell}	Pressure loss coefficient
k_f	Coolant thermal conductivity [W/(mK)]
n	Total number of screen layers
N	Number of pores per unit length, (N=1/(w+d))
Nu_{dp}	Nusselt number based on pore diameter
ΔP	Pressure drop [Pa]
Q	Input heat [W]
q	Heat flux [W/m^3]
R_{BR}	Blockage ratio (=frontal area / free flow area)
Re_{dp}	Reynolds number based on pore diameter
t	Screen layer thickness
$T_{f,bulk}$	Bulk mean temperature of coolant at inlet [K]
T_w	Temperature of bottom face sheet [K]
U_m	Mean coolant velocity at inlet [m/s]
V	volume of wire screen [m^3]
W	Width of testing sample [m]
w	Width of cell opening [m]

Greek

a_{sf}	Surface area density [1/m]
e	Porosity
r	Density of copper made screens [kg/m^3]

$\bar{r}$ Relative density

References

[1] M. F. Ashby, A. G. Evans, N. F. Fleck, L. J. Gibson, J. W. Hutchinson, H. N. G. Wadley, Metal Foams: A Design Guide, Butterworth-Heineman, 2000

[2] D. J. Sypeck, H. N. G. Wadley, Multifunctional Microtruss Laminates: Textile Synthesis and Properties, J. Mater. Res., Vol. 16, No. 3, pp. 890-897, 2001

[3] S. Chiras, D. R. Mumm, A. G. Evans, N. Wicks, J. W. Hutchinson, S. Fichter, K. Dharmasena, H. N. G. Wadley, The Structural Performance of Near-optimized Truss Core Panels, Int. J. Solids and Struc., Vol. 39, pp 4093-4115, 2002

[4] H. N. G. Wadley, Cellular Metals Manufacturing, Advanced Engineering Materials, 2002, in press

[5] T. J. Lu, H. A. Stone, M. F. Ashby, Heat Transfer in Open-Cell Metal Foams, Acta Mater., Vol. 46, pp. 3619-3635, 1998

[6] A. G. Evans, J. W. Hutchinson, N. A. Fleck, M. F. Ashby, H. N. G. Wadley, The Topological Design of Multifunctional Cellular Metals, Progress in Materials Science, Vol. 46, pp. 309-327, 2001

[7] D. R. Mumm, A. G. Evans, D. J. Sypeck, H. N. G. Wadley, On the Performance of Light Weight Metallic Panels Fabricated Using Textile Technology, 2002, submitted for publication

[8] J. C. Armour, J. N. Cannon, Fluid Flow Through Woven Screens, AIChE Journal, Vol. 14, No. 3, pp. 415-421, 1968

[9] W. S. Chang, Porosity and Effective Thermal Conductivity of Wire Screens, ASME Journal of Heat Transfer, Vol. 112, pp. 5-9, 1990

[10] J. R. Sodré, J. A. R. Parise, Friction Factor Determination for Flow Through Finite Wire-Mesh Woven-Screen Matrices, ASME Journal of Fluid Engineering, Vol. 119, pp. 847-851, 1997

[11] D. Mehta, M. A. Hawley, Wall Effect in Packed Columns, I & EC Process Design and Development, Vol. 8, No. 2, pp. 280-282, 1969

[12] S. Ergun, Fluid Flow Trough Packed Columns, Chemical Engineering Progress, Vol. 48, No. 2, pp. 89-94, 1952

[13] F. Duprat, G. Lopez, Comparison of Performance of Heat Regenerators: Relation Between Heat Transfer Efficiency and Pressure Drop, Int. J. of Energy Research, Vol. 25, pp. 319-329, 2001

[14] A. Ahmad, J. Saini, H. Varma, Effect of Geometrical and Thermo-physical Characteristics of Bed Materials on the Enhancement of Thermal Performance of Packed-Bed Solar Air Heaters, Energy Conversion and Management, Vol. 36, pp. 1185-1195, 1995

[15] C. T. Hsu, K. W. Wong, P. Cheng, Effective Stagnant Thermal Conductivity of Wire Screen, J. Thermophysics, Vol. 10, No. 3, pp. 542-545,1996

[16] P. Jiang, M. Li, T. J. Lu, Z. Ren, X. Sun, Convection Heat Transfer in Sintered Porous Plate Channels, Proc. 12th International Conference on Heat Transfer, Grenoble, France, August 2002

[17] T. Kim, A. J. Fuller, H. P. Hodson, and T. J. Lu, An Experimental Study on Thermal Transport in Lightweight Metal Foams at High Reynolds Numbers, Proc. International Symposium of Compact Heat Exchangers, Grenoble, France, pp-227-232, 2002

[18] H. W. Coleman, W. G. Steele, Experimentation and Uncertainty Analysis for Engineers, 2nd Ed. John Wiley & Sons Inc. 1999

[19] T. Kim, C. Y. Zhao, T. J. Lu, H. P. Hodson, Convective Heat Dissipation with Lattice-Frame Materials, Mech. Mater., 2002 (in press)

[20] C. Y. Zhao, T. Kim, T. J. Lu, H. P. Hodson, Modeling on Thermal Transport in Cellular Metal Foams, 8th Joint AIAA/ASME Thermophysics and Heat Transfer Conference, AIAA Paper # 2002-3014, St. Louis, USA, June 2002